

Phase diagram of $SU(2)$ with 2 flavors of dynamical adjoint quarks

Simon Catterall, Department of Physics, Syracuse University, Syracuse, NY 13244, USA
E-mail: smc@phy.syr.edu

Joel Giedt, Department of Physics, Applied Physics and Astronomy, Rensselaer Polytechnic Institute, Troy, NY 12180 USA E-mail: giedtj@rpi.edu

Francesco Sannino, HEP Center, Institute for Physics and Chemistry, University of Southern Denmark, Odense, Denmark. E-mail: sannino@ifk.sdu.edu

Joe Schneible, Department of Physics, Syracuse University, NY 13244. E-mail: jschneib@physics.syr.edu

ABSTRACT: We report on numerical simulations of $SU(2)$ lattice gauge theory with two flavors of light dynamical quarks in the adjoint of the gauge group. The dynamics of this theory is thought to be very different from QCD – the theory exhibiting conformal or near conformal behavior in the infrared. We make a high resolution survey of the phase diagram of this model in the plane of the bare coupling and quark mass on lattices of size $8^3 \times 16$. Our simulations reveal a line of first order phase transitions extending from $\beta = 0$ to $\beta = \beta_c \sim 2.0$. For $\beta > \beta_c$ the phase boundary is no longer first order but continues as the locus of minimum meson mass. For $\beta > \beta_c$ we observe the pion and rho masses along the phase boundary to be light, independent of bare coupling and approximately degenerate. We discuss possible interpretations of these observations and corresponding continuum limits.

KEYWORDS: Lattice gauge theory; higher representations; technicolor; dynamical electroweak symmetry breaking; dynamical fermion simulations.

Contents

1. Introduction	1
2. Summary of the Analytical Results	3
3. Lattice Implementation	4
3.1 Action and simulation algorithm	4
3.2 Meson operators	5
3.3 String tension	5
4. Results	6
5. Discussion	9

1. Introduction

Non-abelian gauge theories at zero temperature and matter density can exist in a number of distinct phases which can be distinguished by the characteristic dependence of the potential energy on distance for two well separated static sources. These different behaviors of the potential energy can be accessed by varying the number of colors and the number of flavors of fermions. The collection of all of these different behaviors, when represented in the flavor-color space, constitutes the *Phase Diagram* of the given gauge theory. Up to possible dualities among different theories it uniquely defines each theory. In [1] the reader will find an up to date review of all of the possible phases for a generic gauge theory.

Knowing the phase diagram of strongly coupled theories has an immediate impact on the construction of sensible extensions of the standard model of particle interactions. Dynamical breaking of the electroweak symmetry is a time-honored example. It is well known that scaled up versions of QCD [2] are ruled out by electroweak precision data.¹

Using fermions in higher dimensional representations of the gauge group opens up many new phenomenological possibilities [4, 5, 6]. There are, in fact, a number of reasons to recommend using higher dimensional representations in the underlying dynamics breaking the electroweak theory: i) The dynamics is generally different from QCD; ii) A near conformal behavior can be reached for a very low number of fermions naturally reducing the contribution

¹The reader will find in [1, 3] an exhaustive review of all of the precision data results from LEP I and II and how they constrain old and new models of dynamical breaking of the electroweak theory.

to precision observables [4]; iii) The spectrum of spin one states of these theories leads to interesting physical processes to be observed at the LHC [7, 8, 9].

An explicit phenomenological realization of this type of model is termed Minimal Walking Technicolor (MWT) [9] and is based on an $SU(2)$ gauge theory coupled to two flavors of adjoint quarks. This model is thought to lie close in theory space to theories with non-trivial infrared fixed points [4, 10]. Indeed it is possible that this theory already exhibits such a fixed point. In the vicinity of such a zero of the beta-function the coupling constant flows slowly or *walks*. Originally such models were introduced to alleviate the flavor changing neutral current problem for extensions of the technicolor theory needed to give mass to the standard model fermions [11, 12, 13, 14]. The MWT is thought to achieve such walking behavior with a minimal number of light (techni)quarks [4]. This is the theory studied numerically in this paper.

Another recent extension of the standard model which has attracted a great deal of interest is unparticle physics [15]. One simply couples a new conformal sector to the standard model. It is natural to identify this sector with a strongly coupled theory featuring an infrared fixed point. Knowledge of the phase diagram is then essential to provide natural ultraviolet completions of unparticle models. Making use of the analytic knowledge of the phase diagram one finds, for example, that it is not easy to construct gauge theories with an infrared fixed point able to produce spinor-type “unparticle stuff” [1].

It is hence crucial to gain information on the phase diagram of strongly interacting gauge theories. Lattice methods and computational resources are now mature enough to provide a “first principles” systematic study of such phase diagrams, with dynamical fermions in the chiral limit on reasonably large lattices. Investigations of representations other than the fundamental have just begun [16, 17, 18, 19], significantly extending older work on very small lattices [20]. Simulation studies of many flavors in the fundamental representation have also become more active of late [21, 22], extending the results of [23, 24].

In the current work we provide a high resolution scan of the mass/coupling phase diagram (not to be confused with colors/flavors/representation discussed above) of $SU(2)$ gauge theory with two (Dirac) flavors of fermions in the adjoint (triplet) representation, using larger lattices and higher statistics than were utilized in our earlier work [16]. We find clear evidence of a phase boundary in the two dimensional plane of bare gauge coupling and quark mass. For $\beta < \beta_c \sim 2.0$ the system undergoes a first order phase transition as this line is crossed. The latent heat of this transition goes to zero for $\beta \rightarrow \beta_c$ while the line continues to larger β as the locus of minimum meson mass. For $\beta < \beta_c$ we see evidence for chiral symmetry breaking and a Goldstone behavior of the pion. Conversely, for $\beta > \beta_c$ the Goldstone behavior $m_\pi^2 \propto m_q$ disappears in a novel way as the system is tuned close to the phase boundary, the string tension in lattice units is so small that we can only bound it from above, and the pion and rho masses drop quickly to values that are degenerate, within statistical errors.

All this behavior is indicative of a theory that is very different from QCD, or even the theories with fundamental flavors that have been studied on the lattice. We will describe the various possible interpretations of the lattice data in the Discussion section at the end of this

work, but here we would like to highlight the most interesting one: all of the lattice data that we have obtained is consistent with either a nontrivial infrared fixed point where the theory becomes conformal, or a theory with an asymptotically free beta function that is very small for the range of scales accessible on our lattice (i.e., the coupling runs so slowly that we cannot start at weak coupling and still have access to the confinement scale on lattice of modest size).

Either way, if this theory were to provide the mechanism of dynamical electroweak symmetry breaking, the phenomenology would be radically different from a QCD-like technicolor scenario, and most likely naive dimensional analysis arguments would not be valid. Thus, the lattice results that we have obtained are quite exciting from this perspective and warrant further studies on larger lattices, which are currently in progress.

In the next section we summarize some of the relevant analytical results. We then describe our lattice model and present our numerical results. Finally, we end with a discussion and interpretation of what we have found from our Monte Carlo study. A full tabulation of the meson masses that we have obtained is presented in Appendices A and B.

2. Summary of the Analytical Results

Dynamical fermion lattice simulations of higher dimensional representations are at an exploratory stage and it is hence useful to compare the results with theoretical expectations obtained using various analytical methods. To gain insight one can now use, for instance, the conjectured all-order beta function for nonsupersymmetric gauge theories [10] together with the constraints from the unitarity of the conformal operators. This method constitutes a step forward with respect to the older approach based on the truncated Schwinger-Dyson equation (SD) [25, 26, 27], which is also referred to as the “ladder approximation” in the literature. In contrast to the ladder approximation, the all-order beta function allows one to determine the fermion mass anomalous dimension for any strongly coupled gauge theory at the infrared fixed point. Anomalous dimensions at fixed points are scheme independent since they represent physical quantities. The analytical phase diagram obtained by this approach, and a comparison of it to recent lattice results [16, 18, 19, 21, 22], is summarized in [1].

In the ladder approximation the $SU(2)$ theory with two Dirac flavors of adjoint fermions should be *just* below the conformal window where the theory develops an infrared fixed point [4]. In the context of this approximation this means that the anomalous dimension of the fermion mass exceeds unity. However, according to the all-order beta function, if the infrared fixed point is actually reached then the anomalous dimension assumes the value $\gamma = 3/4$, where $\gamma = -d \ln m / d \ln \mu$ and m is the running fermion mass. If we take $\gamma = 1$ as the boundary of the conformal window, the all-order beta function suggests that the $SU(2)$ model is conformal in the infrared. However, the constraint coming from the unitarity allows γ to be as large as two before conformality is lost. Thus it is an open question whether or not a nontrivial infrared fixed point exists. As will be seen, the results of our lattice study suggest

that this fixed point may exist, though further investigations will be required to strengthen the case for that conclusion.

It is instructive to compare this theory with the case of the $SU(3)$ gauge theory with two Dirac fermions in the two index symmetric representation. In “theory space” the previous gauge theory and the present one are very close, since the adjoint of $SU(2)$ is equivalent to the two index symmetric representation. Recent lattice results [18] suggest that this theory may have an infrared fixed point, though more studies are needed here too. We note that the ladder approximation predicts that this theory is nearly conformal (*i.e.* walking), and further away from conformality than the $SU(2)$ theory. Also, if one assumes that the theory is conformal in the infrared, then the all-order beta function predicts that the anomalous dimension of the fermion condensate is $\gamma = 1.3$, larger than the value of $3/4$ that was found in the $SU(2)$ case above. If it is true that $SU(3)$ has an infrared fixed point, it follows that the $SU(2)$ theory also has an infrared fixed point, since the screening due to fermions is even greater in the latter case.

As an aside, we note that it is quite interesting that for $SU(3)$ the anomalous dimension γ is larger than unity. If true, this would be quite an important result, since large anomalous dimensions are needed when constructing extended technicolor models that are able to account for the heavy quark masses, as noted in [1]. If the preliminary indications of $\gamma > 1$ hold up to further scrutiny, it would overturn the common lore—but no rigorous theorem—regarding the anomalous dimension of the “quark” bilinear operator.

Other interesting cases to consider are those with eight and twelve Dirac fermions in the fundamental representation of $SU(3)$. The all-order beta function predicts that the conformal window cannot be achieved for a number of flavors less than 8.25 (really, nine once the integer constraint is imposed) for the fundamental representation of $SU(3)$. This is confirmed by the latest lattice results [21, 22]. In that work it was also suggested that the theory with twelve flavors has an infrared fixed point. The prediction of the anomalous dimension of the quark mass operator is then $\gamma = \frac{3}{4}$. Amusingly this theory has the same anomalous dimension as the $SU(2)$ two adjoint flavor theory that we study here (assuming they both possess an infrared fixed point).

3. Lattice Implementation

3.1 Action and simulation algorithm

The lattice action we employ consists of the usual Wilson plaquette term

$$S_G = -\frac{\beta}{2} \sum_x \sum_{\mu > \nu} \text{ReTr} \left(U_\mu(x) U_\nu(x + \hat{\mu}) U_\mu^\dagger(x + \hat{\nu}) U_\nu^\dagger(x) \right) , \quad (3.1)$$

with the link matrices $U_\mu(x)$ in the fundamental representation of $SU(2)$, together with the

Wilson action for two Dirac fermions in the adjoint representation:

$$S_F = -\frac{1}{2} \sum_x \sum_\mu \bar{\psi}(x) (V_\mu(x) (I - \gamma_\mu) \psi(x + \mu) + V_\mu^T(x - \mu) (I + \gamma_\mu) \psi(x - \mu)) \quad (3.2)$$

$$+ \sum_x (m + 4) \sum_x \bar{\psi}(x) \psi(x) . \quad (3.3)$$

Here adjoint links $V_\mu(x)$ are used, which are related to the fundamental links by

$$V_\mu^{ab}(x) = \frac{1}{2} \text{Tr} \left(\sigma^a U_\mu(x) \sigma^b U_\mu^\dagger(x) \right) , \quad (3.4)$$

with σ^a , $a = 1, 2, 3$ the usual Pauli matrices.

We have simulated this theory over a range of gauge couplings $\beta = 1.5 - 3.0$ and bare quark masses m ranging from $-2.0 < m < 0.5$ on $8^3 \times 16$ lattices using the usual Hybrid Monte Carlo algorithm [28]. Typically we have generated between 400 – 2000 $\tau = 1$ HMC trajectories. Antiperiodic boundary conditions were used for the fermions in the time direction (in order to ameliorate problems with exceptional configurations at the for small quark mass), whereas all other boundary conditions are periodic.

All simulations were run on the IBM BlueGene/L SUR machine at Rensselaer over a period of four months. The simulation software used is a recent, BlueGene/L architecture-specific version of the Columbia Physics System, modified such that SU(2) with any number of adjoint (Wilson or domain wall) fermions can be studied. The code has been validated by reproducing the results of [29] for the case of pure super-Yang-Mills. Indeed, the software was developed for a large-scale follow-up study of pure super-Yang-Mills that is in progress [30]. The average compute rate was 70 Gflop/s, on a 128 node partition of the BlueGene/L.

3.2 Meson operators

We estimate the hadron masses by suitable fits to corresponding time sliced averaged correlation functions

$$G_O(t) = \sum_{x,y} \langle \bar{\psi}(x,t) \Gamma_O \psi(x,t) \bar{\psi}(y,0) \Gamma_O \psi(y,0) \rangle \quad (3.5)$$

where $\Gamma_O = \gamma_5$ for the pion and $\Gamma_O = \gamma_\mu$, $\mu = 1, 2, 3$ for the rho (the latter being averaged over spatial directions μ). Errors are estimated by a jackknife procedure in which fits are made to the meson correlators using subsets of the data, the mean and deviation of the resulting mass distribution yielding a mean meson mass and error.

3.3 String tension

We estimate the string tension as a function of lattice scale R from the large distance asymptotic behavior of the Creutz ratio [31]

$$\chi(R, R) = -\ln \frac{W(R, R)W(R-1, R-1)}{W(R, R-1)W(R-1, R)} \sim \sigma a^2. \quad (3.6)$$

Here $W(R, R')$ is the expectation value of the $R \times R'$ Wilson loop and a is the lattice spacing. The asymptotic behavior on the r.h.s. of (3.6) assumes an area law for the Wilson loops. In practice one looks for the Creutz ratios $\chi(R, R)$ to coalesce on an envelope where the area law becomes dominant. This occurs for Ra of order or larger than the scale of confinement $\ell_c = 1/\Lambda$, where Λ is the usual dynamical scale of an asymptotically free gauge theory. In the chiral limit where the fermions are massless, the lattice spacing is a function of the bare lattice coupling $\beta = 4/g^2$, through $a \sim \Lambda^{-1} \exp(-2\pi^2\beta/b)$ where b is the 1-loop beta function coefficient. (Of course this estimate can be improved with high loop results, as has been considered in [17].) Thus since σ and Λ are physical scales, one expects to see an exponentially decreasing envelope for the Creutz ratios. Away from the chiral limit, there is a threshold mass above which the running of the coupling is altered. In that case one would have $a = a(\beta, m)$, where m is the bare fermion mass. Finally, we should note that since we use fundamental links in the Wilson loops, they are not screened by the adjoint fermions, and an area law emerges at scales $Ra > \ell_c$, provided the theory is asymptotically free. On the other hand, if the theory has a nontrivial infrared fixed point, the only scale available is the finite extent of the lattice, $L^3 \times T$ (here, dimensionless quantities). One would therefore expect to see that the Creutz ratio behavior depends strongly on L, T , in contrast to what happens in the confining case where for $\sigma a^2 L^2$ and $\sigma a^2 T^2$ very large the results become independent of L, T .

4. Results

Our results were obtained as a series of bare Wilson fermion mass scans, at fixed bare gauge coupling $\beta = 4/g^2$. Perhaps the simplest observable to consider is the expectation value of the plaquette or action. Fig. 1 shows a series of scans in the “quark” mass for different values of β . (In what follows we will often refer to the elementary fermions as “quarks” and composite states as “pions”, “rhos”, etc. Of course this is only by way of analogy, and we could alternatively prefix these names with “techni-”.) Notice the appearance of a discontinuity for small $\beta < \beta_c \sim 2.0$. The data indicates that a line of first order phase transitions exists for small β . Further support for this conclusion comes from the latent heat, as measured by the jump in the plaquette and displayed in Fig. 2. It appears to vanish as $\beta \rightarrow \beta_c \sim 2.0$. Beyond β_c we observe that the phase boundary continues as the locus of minimum pion and rho meson mass. The natural conclusion is that $\beta_c \approx 2$ is a second order end-point for the line of first order transitions. In Section 5 we will interpret the first order behavior across the phase boundary, at $\beta < \beta_c$, as corresponding to a bulk phase transition in the effective SU(2) gauge theory, in accordance with the well-known combined fundamental/adjoint plaquette action phase diagram [32, 33].

In Fig. 3 we illustrate the behavior of the rho mass $m_\rho a$ by plotting it as a function of the bare Wilson fermion mass ma at three representative points in the phase diagram: $\beta = 1.5$, $\beta = 2.0$ and $\beta = 2.5$. (The full set of rho mass results from our studies is tabulated in Appendix B.) The region of quark mass to the left of the minimum corresponds to an

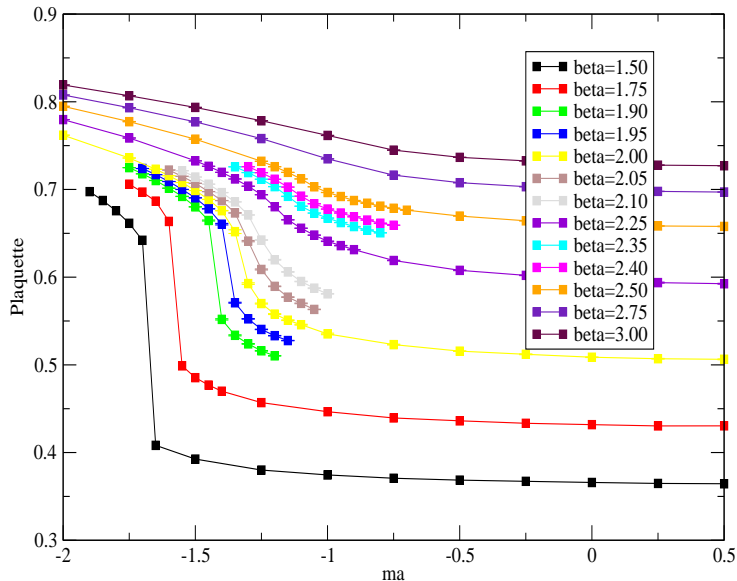


Figure 1: Plaquette expectation values as a function of the bare fermion mass, along lines of constant lattice gauge coupling $\beta = 4/g^2$. It can be seen that $\beta_c \approx 2$ marks a transition, below which a first order phase transition is seen as the quark mass is varied. We therefore find that close to the phase boundary, β_c corresponds to a “bulk” transition, below which only a lattice phase exists. This can be understood in terms of the dynamical generation of an effective adjoint plaquette term in the gauge action, due to the radiative effects of nearly massless adjoint “quarks.” Of course, for masses far enough away from the critical value the renormalization of the gauge action is relatively small and the adjoint term will not lead to a bulk transition.

Aoki phase [34], except that here it is for adjoint Wilson fermions, which was recently studied in [17]². In the case of $\beta \geq 2$, as one approaches the minimum meson mass from above, there is a rapid drop in m_ρ that is inconsistent with a simple linear variation with bare quark mass $m_\rho \propto m - m_c$, as one would see in QCD, or in the case of two fundamental flavors observed in [16] (cf. Fig. 5 of that reference). The data corresponds instead to a form

$$m_\rho \sim (m - m_c)^{1/(1-\epsilon)}, \quad 0 < \epsilon < 1. \quad (4.1)$$

Similar results are obtained for the pion, illustrated for some three values of β in Fig. 4 below. (A full tabulation of pion masses is given in Appendix A.) The figure shows the $(m_\pi a)^2$ as a function of the bare quark mass ma , so it is important to keep in mind that the dependence of the lattice spacing on β, m also enters into the plot. There is clear evidence of a linear Goldstone dependence at strong coupling consistent with chiral symmetry breaking for $\beta < 2.0$. Conversely at $\beta = 2.5$ the data near the phase boundary line is consistent

²Notice that the dependence of the rho mass on bare quark mass appears to depart from linear at strong coupling which we attribute to the proximity of the first order phase transition

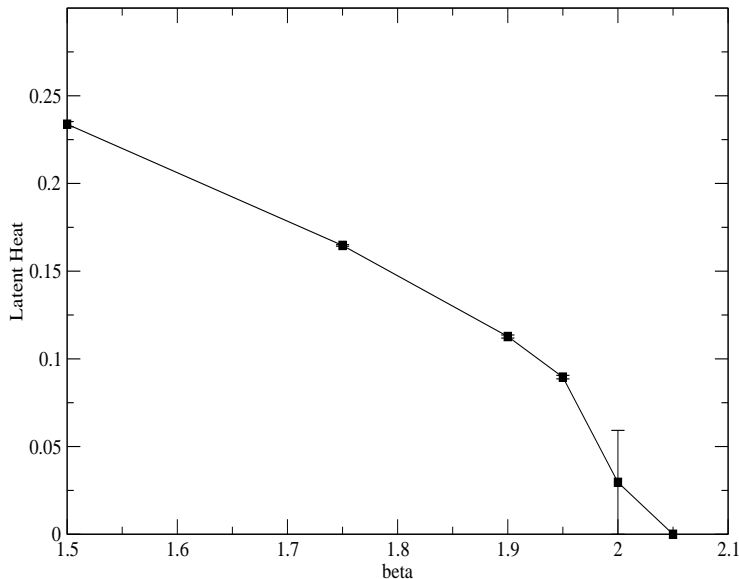


Figure 2: The latent heat, which appears to vanish in the $\beta \rightarrow 2$ limit.

with a simple linear dependence of the pion mass on bare quark mass and chiral symmetry restoration. Again, the pion mass varies very rapidly with bare quark mass close to $\beta = 2.0$. One interpretation, which we will discuss further below, is that the lattice spacing shrinks significantly as one approaches the chiral limit, due to the comparable renormalization of the gauge coupling by gluons and quarks in this model. I.e., the coupling walks when the quarks are very light, and does so over a large range of scales as the quarks approach zero renormalized mass.

The behavior of the pion and rho masses along the entire phase boundary is shown in Fig. 5. Two regimes are seen; a strong coupling phase with a light pion and heavy rho for $\beta < \beta_c \sim 2.0$ and a phase for $\beta > \beta_c$ where the pion and rho are approximately degenerate and independent of the bare coupling. The situation at $\beta \sim \beta_c$ is somewhat unclear as the statistical errors are large there. The phase boundary itself is shown below in Fig. 6.

We have also made estimates of the string tension as measured by Creutz ratios $\chi(R, R)$ [cf. (3.6)] of various sizes. Fig 7 shows a plot of $\chi(R, R)$, $R = 1, \dots, 5$, as a function of β as we move along the phase boundary $m_c(\beta)$. At distances of order or larger than the confinement scale, these ratios should coalesce on the value of σa^2 where σ is the string tension. For $\beta = 1.9, 1.95$ this occurs, as it can be seen that $\chi(4, 4)$ and $\chi(5, 5)$ coincide. For $\beta \geq 2$ the envelope where χ 's begin to converge cannot be seen, but the value of $\chi(5, 5)$ places an upper bound on σa^2 . It may be that much larger R values in $\chi(R, R)$ are needed, which is not possible on the $8^3 \times 16$ lattice that we study here. This would be the case if the lattice spacing a has the very sensitive exponential dependence on β that would be expected from a

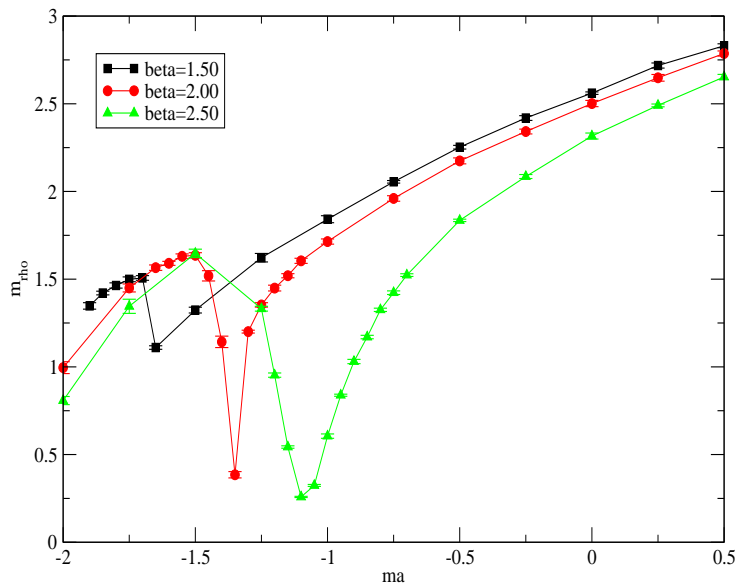


Figure 3: The “rho” mass $m_\rho a$, as a function of the bare Wilson fermion mass m , for three example values of the bare lattice coupling β . Note that as β increases past the critical value $\beta_c \approx 2$, the ρ mass on the phase boundary becomes small on the order of the inverse lattice size $1/L$. This is consistent with the ρ becoming a massless state in the thermodynamic limit

walking theory; for instance in the present theory using 2-loop running one would predict that between $\beta = 2$ and $\beta = 2.1$, σa^2 would decrease by an order of magnitude and between $\beta = 2$ and $\beta = 2.5$ it would decrease by five orders of magnitude. Given the trend in Creutz ratios with R at $\beta = 2$, one can roughly estimate that $\chi(7, 7)$ or $\chi(8, 8)$ may be required before the envelope at this value of β would be seen. This would require a lattice of size $16^3 \times 32$, which we are currently studying. On the other hand, and this is the possibility that we would like to emphasize, it could be that for $\beta \geq 2$ one falls into the basin of attraction for a nontrivial infrared fixed point, and the area law does not hold at any scale.

For $\beta < 2$ one has hints of the envelope, though the large statistical errors due to enhanced fluctuations at small β prevent us from measuring the larger loops needed for $\chi(4, 4)$ and $\chi(5, 5)$. Nevertheless, it would appear that the string tension σ is of order $1/a^2$, consistent with a phase of the theory dominated by lattice artifacts.

In the next section we discuss further the possible interpretations of these observations.

5. Discussion

Generically a lattice gauge theory will have a confining phase at strong bare coupling, and we believe this to be true for the present theory. Typically this is signaled by a non-zero string tension extracted from the asymptotic behavior of Wilson loops, or correlation functions of

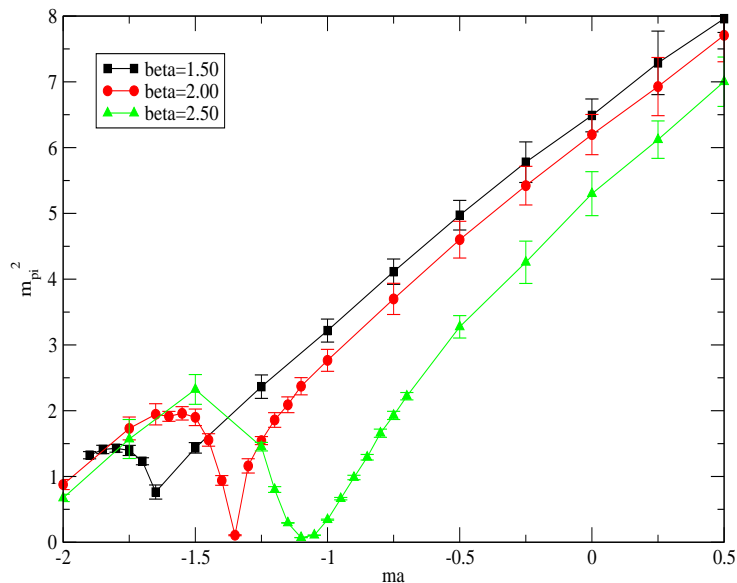


Figure 4: The pion mass squared for example values of β . The very sharp behavior as the bare mass is varied away from the phase boundary near $\beta = 2$ stands in contrast to the rounding that would normally be expected from the effects of the finite size effects. The significant decrease in the slope of the line as one approaches the phase boundary is presumably due to $(m_\pi a)^2/(ma) \sim a$, with $a(\beta, m)$ having a significant m dependence when the fermions are very light. This is particularly true since the contribution of the quarks to the running of the coupling is quite close to that of the gluons.

Wilson/Polyakov lines. However at strong coupling the lattice theory will be dominated by lattice artifacts. For instance, from Fig. 7 on sees that at $\beta < \beta_c \approx 2$, the Creutz ratios indicate that $\sigma a^2 = \mathcal{O}(1)$, so that for small β (strong coupling) the string tension, and hence scale of confinement, is of the same scale as the lattice spacing a . Similarly, in Fig. 3 on sees that for $\beta = 1.5$ we obtain $m_\rho a \geq 1$, indicating that the rho also lies at the ultraviolet cutoff scale.

To understand whether this confining strongly coupled phase survives the continuum limit it is necessary to examine the behavior of, say, a Wilson loop, as the lattice spacing is sent to zero holding the area of the Wilson loop fixed in physical units. For a theory exhibiting asymptotic freedom this is accomplished by increasing β . In the case of QCD and on an infinite lattice this process can be continued indefinitely until we end up at the fixed point $\beta = \infty$, thereby removing the ultraviolet cutoff. However it is possible that this procedure is interrupted by the presence of a first order phase transition at some finite bare coupling—so that the signal of confinement at strong coupling is not a property of the continuum theory. This appears to happen in this model, in the vicinity of the first order line. That is, our results indicate that the strong coupling phase at $\beta < \beta_c$ is not continuously connected to a phase with a continuum limit.

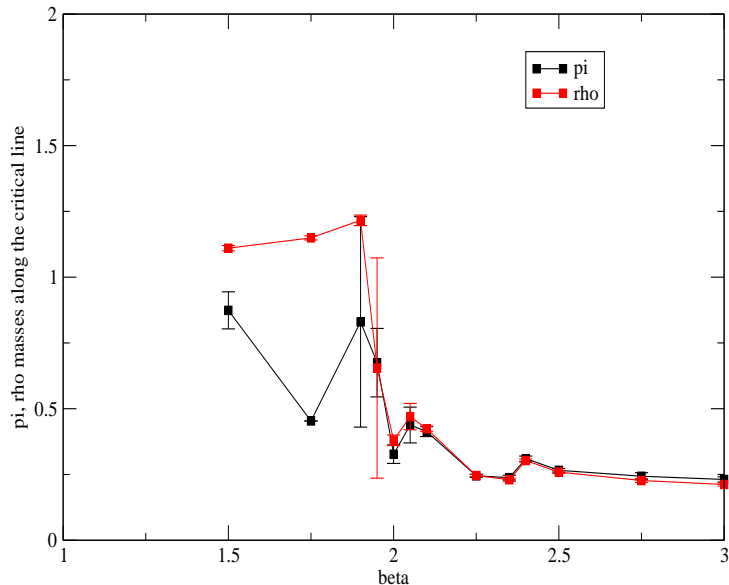


Figure 5: Pion and rho masses along the phase boundary. Note that they become degenerate for $\beta \gtrsim 2$.

On the other hand, it does appear that one can move smoothly into a continuum phase if one starts sufficiently far away from phase boundary. In fact, this must be true since for large enough mass the theory is an arbitrarily good approximation of the quenched theory with just the Wilson plaquette action in the fundamental representation. Since that theory does not have a discontinuity separating the strong and weak coupling phases, we know that this is also true in our theory in this quenched limit.

It is also possible that the a continuum theory with massless quarks may be obtained by tuning the bare quark mass in the regime $\beta > \beta_c$. The fact that the minimum meson mass appears to scale with the inverse lattice size is consistent with this.

All of this can be understood in terms of radiative effects of two flavors of adjoint fermions. If the fermions are very light, they will generate a large adjoint plaquette term when they are integrated out to obtain the long wavelength effective theory. As mentioned briefly above, it is known that a first order transition occurs in the adjoint plaquette action theory [32] and that in the mixed fundamental/adjoint plaquette theory there is a first order transition line when the adjoint term is sufficiently large [33]. The interpretation of our results is therefore clear: if the quarks are approximately massless, the adjoint fermions lead to a large effective adjoint plaquette term, conventionally characterized by the coefficient β_A . As one passes through the phase boundary at small fundamental plaquette action coupling β , one is actually moving back and forth across the first order line in the β - β_A plane. Since in the quenched fundamental/adjoint theory the first order line only exists for $\beta < 1.6, \beta_A > 0.7$, we

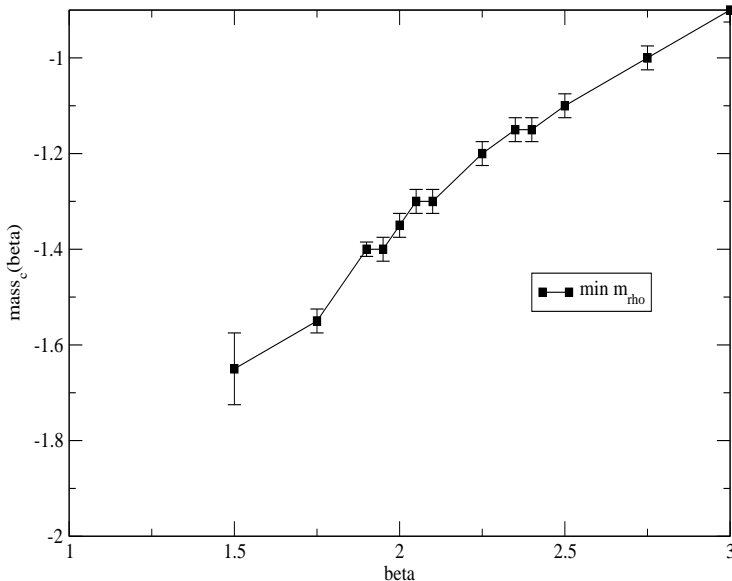


Figure 6: Here, the phase boundary is extracted from the minimum of rho mass at each β .

can understand why we too see that the first order behavior disappears for sufficiently large β or mass m . The fact that the transition in our theory happens instead at $\beta_c \approx 2$ would again be due to the radiative effects of the fermions, which will also renormalize β .

Since in a walking technicolor scenario we are interested in the theory with massless fermions, the phase of the lattice theory that is relevant for continuum physics is the phase where $\beta > \beta_c$. For $\beta \rightarrow \infty$ we expect that the theory is driven to the asymptotically free fixed point known to exist in perturbation theory. However the behavior of the theory in the infrared is less clear. If the theory admits a new conformal fixed point then one expects that this will govern the long distance physics of the model and long distance features of the theory will be insensitive to the bare lattice coupling. In addition such a theory has no intrinsic scale, so that the only scales would be the lattice volume and the temperature. It follows that both the string tension and meson masses would scale to zero in the zero temperature, thermodynamic limit. This sort of behavior is certainly consistent with what we see in the phase $\beta > \beta_c$ along the line of minimum meson mass $m = m_c(\beta)$. Thus, our findings are *consistent with the appearance of a new conformal fixed point in this theory*, though they also leave open the possibility of a walking theory.

However, one must be careful in drawing the conclusion that a nontrivial infrared fixed point exists. To take the continuum limit along the critical line requires tuning the bare coupling β with lattice spacing a such that finite size effects are under control. If this running $\beta(a)$ is sufficiently slow it can lead to extreme sensitivity in the dependence of the lattice spacing on bare coupling, when inverted to give $a = a(\beta)$. As was discussed in relation

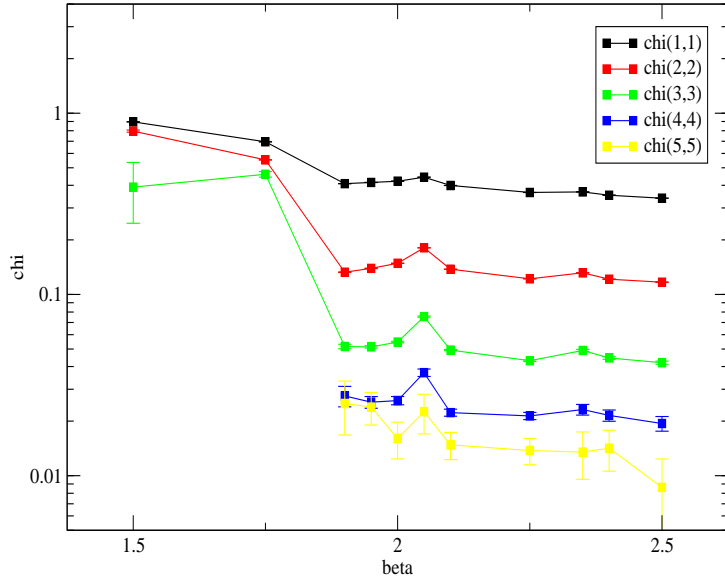


Figure 7: Here we show the Creutz ratios along the phase boundary corresponding to minimum meson masses. For $\beta = 1.9, 1.95$ the envelope that determines σa^2 can be seen from $\chi(4, 4)$ and $\chi(5, 5)$, since they coincide. For $\beta \geq 2$ the envelope where χ 's begin to coalesce cannot be seen, though the value of $\chi(5, 5)$ places an upper bound on σa^2 . For $\beta < 2$ there is some indication of an envelope, though large statistical errors prevent us from measuring the larger loops needed for $\chi(4, 4)$ and $\chi(5, 5)$.

to the Creutz ratio data above, small increases in the β would yield huge decreases in the lattice spacing. It is difficult to analyze such changes of scale on a relatively small lattice. In particular, large finite size effects can mask the true infinite volume, zero temperature physics. For example, the physical box size can become so small that the system deconfines and looks quasi-free, which would also be consistent with our data. In effect, the physics is indeed being dominated by a conformal fixed point—not a new infrared stable point but the usual infrared unstable asymptotically free fixed point. To distinguish amongst the possibilities will require larger lattices and a thorough study of finite size effects, so one must be cautious in interpreting our findings thus far.

Another way of restating this is that any theory whose coupling runs very slowly with scale will necessarily generate a dynamical mass scale in lattice units (e.g., $a\Lambda$), which is very small for a weak bare coupling. To distinguish a confining theory with a small scale from a theory with a non-trivial infrared fixed point will then necessitate simulations on lattices which are significantly bigger, in lattice units, than the inverse of this small mass scale, which is a hard problem. And, indeed, on small lattices the physics will be governed by the usual ultraviolet fixed point corresponding to asymptotic freedom. On the other hand, simulations on larger lattices would allow us to perform a “step-scaling” analysis, in order to extrapolate to the infinite lattice volume behavior. We have begun studies of $16^3 \times 32$ lattices with the

purpose of distinguishing between the walking and conformal scenarios that we have just described.

Finally we would like to conclude by discussing a possible phase diagram which might be relevant in the situation where the theory does indeed contain a new conformal fixed point. Fig. 8 shows a cartoon of fixed points and possible RG flows for this model projected to the plane of bare coupling constants (β, m) . The arrows denote the flow of couplings under *increases* in length scale corresponding, for example, to a blocking transformation. The theory certainly contains the usual infrared unstable fixed point corresponding to $(\beta, ma) = (\infty, 0)$. A critical line corresponding to massless quarks extends out of this fixed point to smaller β or stronger coupling. If a conformal fixed point exists it should form a sink for these flows as shown.

In the picture we also show as a dashed line the line of first order phase transitions. Our data supports the conjecture that this line ends on a critical point corresponding to another infrared unstable fixed point.

Furthermore, our results are consistent with the first order line and the critical line joining together at the critical endpoint. Any putative conformal fixed point would then serve as a infrared sink for massless flows out of these fixed points as shown³.

Notice that all these fixed points are also unstable in the direction orthogonal to the critical line; i.e. under a mass deformation. Recognizing this fact actually allows us to draw a RG flow that would automatically permit a *walking dynamics* even in a theory inside the conformal window. One merely allows the theory to start near one of ultraviolet fixed points with a small but non-zero mass. Under blocking such a trajectory would flow initially towards the conformal fixed point in the vicinity of which the flow would slow before eventually flowing out along a direction corresponding to a mass deformation. Of course a walking scenario that introduces a mass for the fermions is not what is desired when trying to use the theory studied here for breaking the electroweak symmetry dynamically. Nevertheless, the possibility of a nontrivial infrared fixed point in the present theory would be interesting in its own right. However, there are technicolor models which make use of different gauge dynamics realizing this possibility as explained in [35, 36].

In conclusion, we have found that the present theory at critical fermion mass either has a very slowly running gauge coupling (walking) or a nontrivial infrared fixed point (conformal). The behavior is drastically different from theories that do not sit near the conformal window. However, special difficulties emerge in the present theory due to extreme sensitivity of the lattice spacing on the bare gauge coupling, due to the slow running. Studies on larger lattices and a careful step-scaling analysis is needed, and indeed underway, in order to clarify these issues.

Acknowledgments

Catterall is supported in part by DOE grant DE-FG02-85ER40237. The authors would like to

³Many thanks to Ben Svetitsky for illuminating discussions of these issues

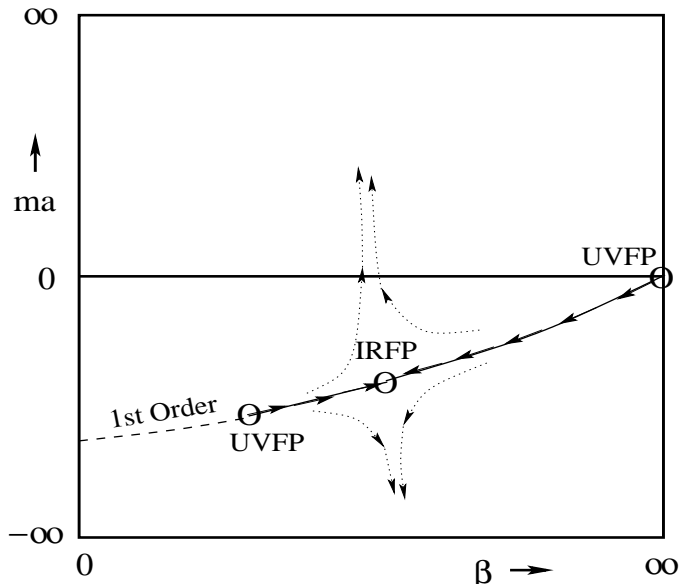


Figure 8: Here we provide a cartoon of renormalization group flows, in order to illustrate what may occur if the present theory has a nontrivial infrared fixed point. The “UV” point on the right corresponds to $(\beta, ma) = (\infty, 0)$, the usual infrared unstable fixed point. On the other hand, “CFP” indicates a putative nontrivial infrared fixed point where the theory is conformal. Flows under a blocking transformation are indicated by arrows along the line of critical masses. Away from this line the theory will flow to a quenched fixed point. The infrared sink is located at the far left-hand side, presumably $(\beta, ma) = (0, -2)$ based on Fig. 6.

acknowledge useful conversations with George Fleming. JG expresses appreciation to Pavlos Vranas for providing a copy of the code that was used in [29], which was used as a basis for the modifications to the current version of the Columbia Physics System. At various points JG also benefited from technical assistance provided by Chulwoo Jung (Brookhaven National Lab) and Adam Todorski (SCOREC and CCNI at Rensselaer). The computational efforts on this project, which utilized the SUR BlueGene/L at Rensselaer, were supported by NSF grant 0420703 entitled “MRI: Acquisition of Infrastructure for Research in Grid Computing and Multiscale Systems Computation” and a gift by the IBM Corporation of a BlueGene/L computer. JG acknowledges support from Rensselaer faculty development funds.

Appendix A: Pion masses

m	pion	error
0.50	2.821	0.013
0.25	2.699	0.033
0.00	2.547	0.019
-0.25	2.403	0.026
-0.50	2.229	0.022
-0.75	2.028	0.023
-1.00	1.793	0.027
-1.25	1.538	0.037
-1.50	1.197	0.027
-1.65	0.873	0.070
-1.70	1.109	0.021
-1.75	1.181	0.027
-1.80	1.195	0.020
-1.85	1.187	0.022
-1.90	1.150	0.020
Pion masses for $\beta = 1.50$.		

m	pion	error
0.50	2.802	0.019
0.25	2.693	0.018
0.00	2.527	0.029
-0.25	2.370	0.029
-0.50	2.200	0.032
-0.75	1.999	0.024
-1.00	1.744	0.041
-1.25	1.481	0.033
-1.40	1.242	0.012
-1.45	1.161	0.017
-1.50	1.061	0.015
-1.55	0.951	0.014
-1.60	0.711	0.048
-1.65	1.304	0.029
-1.70	1.312	0.017
-1.75	1.291	0.020
Pion masses for $\beta = 1.75$.		

m	pion	error
-1.20	1.457	0.011
-1.25	1.385	0.012
-1.30	1.305	0.010
-1.35	1.195	0.011
-1.40	1.048	0.015
-1.45	0.82	0.42
-1.50	1.250	0.026
-1.55	1.351	0.016
-1.60	1.380	0.0075
-1.65	1.386	0.016
-1.70	1.360	0.012
-1.75	1.3367	0.0079
Pion masses for $\beta = 1.90$.		

m	pion	error
-1.15	1.492	0.014
-1.20	1.430	0.016
-1.25	1.340	0.018
-1.30	1.229	0.018
-1.35	1.094	0.027
-1.40	0.67	0.13
-1.45	1.146	0.025
-1.50	1.320	0.016
-1.55	1.392	0.020
-1.60	1.402	0.018
-1.65	1.378	0.026
-1.70	1.358	0.028
Pion masses for $\beta = 1.95$.		

m	pion	error
-1.05	1.550	0.015
-1.10	1.466	0.018
-1.15	1.384	0.012
-1.20	1.249	0.025
-1.25	1.041	0.028
-1.30	0.437	0.068
-1.35	0.693	0.014
-1.40	1.119	0.017
-1.45	1.322	0.020
-1.50	1.409	0.027
-1.55	1.416	0.032
-1.60	1.428	0.012
Pion masses for $\beta = 2.05$.		

m	pion	error
-1.00	1.569	0.014
-1.05	1.488	0.012
-1.10	1.385	0.025
-1.15	1.254	0.022
-1.20	1.062	0.038
-1.25	0.592	0.043
-1.30	0.413	0.018
-1.35	0.915	0.021
-1.40	1.228	0.016
-1.45	1.386	0.028
-1.50	1.419	0.017
-1.55	1.441	0.017
Pion masses for $\beta = 2.10$.		

m	pion	error
0.50	2.776	0.026
0.25	2.632	0.031
0.00	2.489	0.024
-0.25	2.328	0.027
-0.50	2.144	0.030
-0.75	1.923	0.032
-1.00	1.662	0.030
-1.10	1.540	0.027
-1.15	1.445	0.028
-1.20	1.363	0.029
-1.25	1.243	0.019
-1.30	1.077	0.046
-1.35	0.327	0.035
-1.40	0.969	0.039
-1.45	1.247	0.030
-1.50	1.378	0.033
-1.55	1.399	0.025
-1.60	1.383	0.019
-1.65	1.394	0.041
-1.75	1.315	0.050
-2.00	0.936	0.043
Pion masses for $\beta = 2.00$.		

m	pion	error
0.50	2.735	0.025
0.25	2.582	0.023
0.00	2.448	0.039
-0.25	2.254	0.030
-0.50	2.013	0.035
-0.75	1.733	0.041
-0.90	1.488	0.018
-0.95	1.392	0.019
-1.00	1.265	0.022
-1.05	1.112	0.026
-1.10	0.889	0.032
-1.15	0.571	0.026
-1.20	0.245	0.0058
-1.25	0.5721	0.0054
-1.30	1.018	0.017
-1.35	1.283	0.020
-1.40	1.421	0.021
-1.45	1.476	0.025
-1.50	1.494	0.026
-1.75	1.309	0.052
-2.00	0.903	0.072
Pion masses for $\beta = 2.25$.		

m	pion	error
-0.80	1.520	0.021
-0.85	1.414	0.030
-0.90	1.303	0.015
-0.95	1.171	0.022
-1.00	0.989	0.016
-1.05	0.787	0.026
-1.10	0.497	0.015
-1.15	0.2383	0.0085
-1.20	0.499	0.011
-1.25	0.882	0.032
-1.30	1.193	0.026
-1.35	1.388	0.019

Pion masses for $\beta = 2.35$.

m	pion	error
-0.75	1.525	0.023
-0.80	1.441	0.039
-0.85	1.322	0.026
-0.90	1.187	0.047
-0.95	1.049	0.029
-1.00	0.859	0.047
-1.05	0.623	0.030
-1.10	0.319	0.012
-1.15	0.310	0.011
-1.20	0.634	0.024
-1.25	0.998	0.029
-1.30	1.286	0.031

Pion masses for $\beta = 2.40$.

m	pion	error
0.50	2.646	0.026
0.25	2.474	0.023
0.00	2.302	0.031
-0.25	2.063	0.037
-0.50	1.809	0.025
-0.70	1.490	0.012
-0.75	1.388	0.016
-0.80	1.287	0.018
-0.85	1.136	0.016
-0.90	0.992	0.017
-0.95	0.814	0.013
-1.00	0.585	0.012
-1.05	0.3278	0.0089
-1.10	0.2660	0.0069
-1.15	0.5422	0.0066
-1.20	0.895	0.027
-1.25	1.205	0.022
-1.50	1.524	0.048
-1.75	1.252	0.094
-2.00	0.820	0.040

Pion masses for $\beta = 2.50$.

m	pion	error
0.50	2.556	0.030
0.25	2.383	0.037
0.00	2.177	0.031
-0.25	1.916	0.034
-0.50	1.569	0.040
-0.65	1.252	0.028
-0.70	1.109	0.039
-0.75	1.002	0.049
-0.80	0.860	0.033
-0.85	0.686	0.033
-0.90	0.494	0.020
-0.95	0.3026	0.0092
-1.00	0.243	0.013
-1.05	0.428	0.017
-1.10	0.736	0.020
-1.15	1.040	0.040
-1.20	1.273	0.044
-1.25	1.448	0.051
-1.30	1.563	0.036
-1.35	1.579	0.042
-1.50	1.529	0.035
-1.75	1.260	0.061
-2.00	0.777	0.032

Pion masses for $\beta = 2.75$.

m	pion	error
0.50	2.482	0.018
0.25	2.275	0.023
0.00	2.019	0.030
-0.25	1.731	0.041
-0.50	1.340	0.050
-0.60	1.064	0.045
-0.65	0.941	0.045
-0.70	0.799	0.050
-0.75	0.641	0.022
-0.80	0.496	0.033
-0.85	0.330	0.014
-0.90	0.231	0.010
-1.00	0.327	0.020
-1.05	0.541	0.013
-1.10	0.823	0.039
-1.15	1.100	0.047
-1.20	1.357	0.042
-1.25	1.488	0.058
-1.30	1.572	0.021
-1.50	1.441	0.35
-1.75	1.279	0.045
-2.00	0.690	0.024
Pion masses for $\beta = 3.00$.		

Appendix B: Rho masses

m	rho	error
0.50	2.830	0.011
0.25	2.718	0.014
0.00	2.5605	0.0070
-0.25	2.418	0.013
-0.50	2.252	0.010
-0.75	2.0551	0.0072
-1.00	1.841	0.019
-1.25	1.622	0.024
-1.50	1.323	0.016
-1.65	1.110	0.010
-1.70	1.506	0.013
-1.75	1.499	0.013
-1.80	1.463	0.015
-1.85	1.420	0.010
-1.90	1.347	0.018
Rho masses for $\beta = 1.50$.		

m	rho	error
0.50	2.8119	0.0074
0.25	2.7012	0.0080
0.00	2.5366	0.0093
-0.25	2.387	0.013
-0.50	2.221	0.025
-0.75	2.029	0.014
-1.00	1.796	0.016
-1.25	1.557	0.017
-1.40	1.3633	0.0051
-1.45	1.302	0.012
-1.50	1.221	0.0099
-1.55	1.149	0.0078
-1.60	1.389	0.28
-1.65	1.567	0.015
-1.70	1.530	0.014
-1.75	1.4803	0.0092
Rho masses for $\beta = 1.75$.		

m	rho	error
-1.20	1.534	0.0073
-1.25	1.474	0.020
-1.30	1.428	0.022
-1.35	1.344	0.018
-1.40	1.215	0.017
-1.45	1.247	0.058
-1.50	1.560	0.045
-1.55	1.620	0.011
-1.60	1.596	0.020
-1.65	1.569	0.018
-1.70	1.526	0.032
-1.75	1.474	0.014
Rho masses for $\beta = 1.90$.		

m	rho	error
-1.15	1.5674	0.0059
-1.20	1.513	0.012
-1.25	1.439	0.011
-1.30	1.351	0.014
-1.35	1.2269	0.0099
-1.40	0.65	0.41
-1.45	1.408	0.018
-1.50	1.6033	0.0091
-1.55	1.635	0.010
-1.60	1.6084	0.0078
-1.65	1.564	0.013
-1.70	1.527	0.012
Rho masses for $\beta = 1.95$.		

m	rho	error
-1.05	1.6170	0.0077
-1.10	1.542	0.011
-1.15	1.4678	0.0046
-1.20	1.344	0.012
-1.25	1.157	0.012
-1.30	0.470	0.048
-1.35	0.754	0.011
-1.40	1.329	0.012
-1.45	1.597	0.013
-1.50	1.6527	0.0066
-1.55	1.627	0.010
-1.60	1.604	0.012
Rho masses for $\beta = 2.05$.		

m	rho	error
-1.00	1.6278	0.0044
-1.05	1.5596	0.0050
-1.10	1.461	0.011
-1.15	1.346	0.012
-1.20	1.162	0.015
-1.25	0.645	0.031
-1.30	0.424	0.010
-1.35	1.042	0.029
-1.40	1.4635	0.0093
-1.45	1.647	0.016
-1.50	1.644	0.011
-1.55	1.626	0.011
Rho masses for $\beta = 2.10$.		

m	rho	error
0.50	2.786	0.014
0.25	2.647	0.019
0.00	2.501	0.017
-0.25	2.341	0.013
-0.50	2.174	0.017
-0.75	1.960	0.015
-1.00	1.714	0.014
-1.10	1.604	0.014
-1.15	1.519	0.011
-1.20	1.449	0.016
-1.25	1.353	0.012
-1.30	1.201	0.0081
-1.35	0.384	0.018
-1.40	1.142	0.032
-1.45	1.519	0.029
-1.50	1.635	0.014
-1.55	1.630	0.013
-1.60	1.590	0.011
-1.65	1.565	0.015
-1.75	1.449	0.022
-2.00	0.995	0.033
Rho masses for $\beta = 2.00$.		

m	rho	error
0.50	2.739	0.012
0.25	2.597	0.014
0.00	2.456	0.025
-0.25	2.276	0.015
-0.50	2.038	0.013
-0.75	1.774	0.027
-0.90	1.538	0.013
-0.95	1.452	0.012
-1.00	1.331	0.010
-1.05	1.1794	0.0080
-1.10	0.953	0.023
-1.15	0.606	0.021
-1.20	0.2456	0.0035
-1.25	0.5973	0.0058
-1.30	1.132	0.012
-1.35	1.497	0.018
-1.40	1.654	0.012
-1.45	1.683	0.010
-1.50	1.671	0.021
-1.75	1.420	0.032
-2.00	0.919	0.054
Rho masses for $\beta = 2.25$.		

m	rho	error
-0.80	1.5653	0.0088
-0.85	1.459	0.017
-0.90	1.3524	0.0067
-0.95	1.226	0.011
-1.00	1.039	0.016
-1.05	0.830	0.028
-1.10	0.519	0.017
-1.15	0.230	0.0058
-1.20	0.5212	0.0080
-1.25	0.951	0.017
-1.30	1.364	0.029
-1.35	1.612	0.013

Rho masses for $\beta = 2.35$.

m	rho	error
-0.75	1.566	0.013
-0.80	1.481	0.018
-0.85	1.366	0.016
-0.90	1.228	0.019
-0.95	1.100	0.029
-1.00	0.895	0.040
-1.05	0.645	0.016
-1.10	0.320	0.013
-1.15	0.3028	0.0058
-1.20	0.6610	0.0094
-1.25	1.099	0.019
-1.30	1.471	0.020

Rho masses for $\beta = 2.40$.

m	rho	error
0.50	2.652	0.014
0.25	2.4906	0.0077
0.00	2.315	0.017
-0.25	2.085	0.011
-0.50	1.8351	0.0068
-0.70	1.5231	0.0075
-0.75	1.422	0.010
-0.80	1.3252	0.0094
-0.85	1.1699	0.0097
-0.90	1.030	0.012
-0.95	0.8384	0.0059
-1.00	0.605	0.012
-1.05	0.3239	0.0055
-1.10	0.2584	0.0033
-1.15	0.5430	0.0067
-1.20	0.952	0.012
-1.25	1.331	0.013
-1.50	1.647	0.024
-1.75	1.345	0.040
-2.00	0.807	0.023

Rho masses for $\beta = 2.50$.

m	rho	error
0.50	2.563	0.0057
0.25	2.390	0.019
0.00	2.190	0.012
-0.25	1.926	0.025
-0.50	1.597	0.018
-0.65	1.282	0.027
-0.70	1.121	0.028
-0.75	1.016	0.031
-0.80	0.900	0.019
-0.85	0.689	0.030
-0.90	0.4899	0.0078
-0.95	0.2935	0.0099
-1.00	0.2271	0.0073
-1.05	0.4207	0.0071
-1.10	0.742	0.011
-1.15	1.088	0.041
-1.20	1.417	0.033
-1.25	1.638	0.030
-1.30	1.740	0.019
-1.35	1.736	0.023
-1.50	1.636	0.024
-1.75	1.310	0.026
-2.00	0.761	0.018

Rho masses for $\beta = 2.75$.

m	rho	error
0.50	2.490	0.010
0.25	2.281	0.011
0.00	2.028	0.015
-0.25	1.750	0.017
-0.50	1.358	0.024
-0.60	1.069	0.028
-0.65	0.953	0.016
-0.70	0.807	0.032
-0.75	0.629	0.011
-0.80	0.488	0.015
-0.85	0.317	0.012
-0.90	0.2123	0.0060
-0.95	0.305	0.011
-1.00	0.527	0.013
-1.05	0.835	0.018
-1.10	1.147	0.032
-1.15	1.465	0.033
-1.20	1.652	0.033
-1.25	1.738	0.025
-1.30	1.764	0.020
-1.50	1.621	0.022
-1.75	1.301	0.031
-2.00	0.681	0.015
Rho masses for $\beta = 3.00$.		

References

- [1] F. Sannino, arXiv:0804.0182 [hep-ph].
- [2] S. Weinberg, Phys. Rev. D **19**, 1277 (1979); L. Susskind, Phys. Rev. D **20**, 2619 (1979).
- [3] R. Foadi, M. T. Frandsen and F. Sannino, arXiv:0712.1948 [hep-ph].
- [4] F. Sannino and K. Tuominen, Phys. Rev. D **71** (2005) 051901 [arXiv:hep-ph/0405209].
- [5] D. D. Dietrich, F. Sannino and K. Tuominen, Phys. Rev. D **72** (2005) 055001 [arXiv:hep-ph/0505059]; *ibid* Phys. Rev. D **73** (2006) 037701.
- [6] D. D. Dietrich and F. Sannino, Phys. Rev. D **75**, 085018 (2007) [arXiv:hep-ph/0611341].
- [7] T. Appelquist and F. Sannino, Phys. Rev. D **59**, 067702 (1999) [arXiv:hep-ph/9806409].
- [8] T. Appelquist, P. S. Rodrigues da Silva and F. Sannino, Phys. Rev. D **60**, 116007 (1999) [arXiv:hep-ph/9906555].
- [9] R. Foadi, M. T. Frandsen, T. A. Rytto and F. Sannino, Phys. Rev. D **76**, 055005 (2007) [arXiv:0706.1696 [hep-ph]].
- [10] T. A. Rytto and F. Sannino, arXiv:0711.3745 [hep-th].
- [11] E. Eichten and K. D. Lane, Phys. Lett. B **90**, 125 (1980).
- [12] B. Holdom, Phys. Rev. D **24**, 1441 (1981).
- [13] K. Yamawaki, M. Bando and K. i. Matumoto, Phys. Rev. Lett. **56**, 1335 (1986).
- [14] T. W. Appelquist, D. Karabali and L. C. R. Wijewardhana, Phys. Rev. Lett. **57**, 957 (1986).
- [15] H. Georgi, arXiv:hep-ph/0703260.
- [16] S. Catterall and F. Sannino, Phys. Rev. D **76**, 034504 (2007) [arXiv:0705.1664 [hep-lat]].
- [17] L. Del Debbio, M. T. Frandsen, H. Panagopoulos and F. Sannino, arXiv:0802.0891 [hep-lat].
- [18] Y. Shamir, B. Svetitsky and T. DeGrand, arXiv:0803.1707 [hep-lat].
- [19] L. Del Debbio, A. Patella and C. Pica, arXiv:0805.2058 [hep-lat].
- [20] J. Kogut, H. Wyld and D. Sinclair Phys. Rev. Lett. **54**:1980,1985.
- [21] T. Appelquist, G. T. Fleming and E. T. Neil, Phys. Rev. Lett. **100**, 171607 (2008) [arXiv:0712.0609 [hep-ph]].
- [22] A. Deuzeman, M. P. Lombardo and E. Pallante, arXiv:0804.2905 [hep-lat].
- [23] B. Mawhinney, hep-lat/9705030
- [24] Y. Iwasaki, K. Kanaya, S. Kaya, S. Sakai and T. Yoshie, Phys. Rev. D **69** (2004) 014507 [arXiv:hep-lat/0309159].
- [25] T. Appelquist, K. D. Lane and U. Mahanta, Phys. Rev. Lett. **61** (1988) 1553.
- [26] A. G. Cohen and H. Georgi, Nucl. Phys. B **314** (1989) 7.
- [27] V. A. Miransky and K. Yamawaki, Phys. Rev. D **55**, 5051 (1997) [Erratum-*ibid.* D **56**, 3768 (1997)] [arXiv:hep-th/9611142].

- [28] S. Duane, A. Kennedy, B. Pendleton and D. Roweth, Phys. Lett. B195B (1987) 216.
- [29] G. T. Fleming, J. B. Kogut and P. M. Vranas, Phys. Rev. D **64** (2001) 034510 [arXiv:hep-lat/0008009].
- [30] J. Giedt, R. Brower, S. Catterall, G. T. Fleming, P. Vranas, in progress.
- [31] M. Creutz, Phys. Rev. Lett. **45** (1980) 313.
- [32] J. Greensite and B. Lautrup, Phys. Rev. Lett. **47** (1981) 9.
- [33] G. Bhanot and M. Creutz, Phys. Rev. D **24** (1981) 3212.
- [34] S. Aoki, Phys. Rev. D **30** (1984) 2653; **33** (1986) 239; **34** (1986) 3170; Phys. Rev. Lett. **57** (1986) 3136; Nucl. Phys. Proc. Suppl. **60A** (1998) 206 [arXiv:hep-lat/9707020].
- [35] F. Sannino, arXiv:0806.3575 [hep-ph].
- [36] M. A. Luty, arXiv:0806.1235 [hep-ph].